

PII: 0017-9310(97)00165-8

# Experimental study of aspect ratio effects on longitudinal vortex flow in mixed convection of air in a horizontal rectangular duct

M. Y. CHANG and T. F. LIN†

Department of Mechanical Engineering, National Chiao Tung University, Hsinchu, Taiwan

(Received 22 January 1997 and in final form 28 May 1997)

**Abstract**—Combined flow visualization and temperature measurement were carried out to investigate the effects of the aspect ratio on the spatial and temporal characteristics of the longitudinal vortex air flow in a bottom heated horizontal rectangular duct. In the experiment, the Reynolds number was varied from 2.5 to 50, the Rayleigh number from 3000 to 20,000 and the aspect ratio from 2 to 12, covering the steady and unsteady longitudinal vortex flows. The results indicated that the spatial vortex flow structure in a low aspect ratio duct is similar to that in a high aspect ratio duct with the central portion of the wider duct around  $x = A/2$  removed, but the unstable vortex flow at high  $Re$  and  $Ra$  can be stabilized when the aspect ratio is reduced. Besides, in a high aspect ratio duct ( $A \geq 8$ ) a reduction in the Reynolds number causes the flow to change from steady to unsteady state with more frequent roll splitting and merging. While in a low aspect ratio duct ( $A \leq 6$ ) at decreasing  $Re$  the roll cross-section exhibits cyclic expansion and contraction in time and the longitudinal rolls become snaking and time periodic in the downstream portion of the duct. At a higher buoyancy-to-inertia ratio the snaking motion of the rolls gets more intensive and is initiated at a shorter distance from the duct inlet. When the value of the aspect ratio is an odd number, it was found that there are still an even number of rolls induced in the duct. The transition from steady to time-dependent state at increasing buoyancy-to-inertia ratio is subcritical in a high aspect ratio duct ( $A \geq 8$ ). However, in a low aspect ratio duct ( $A \leq 6$ ) there exists a finite range of the buoyancy-to-inertia ratio for the appearance of the time-periodic snaking vortex flow. Finally, the measured oscillation frequencies of the time periodic snaking vortex flow were correlated. © 1997 Elsevier Science Ltd.

## 1. INTRODUCTION

The buoyancy driven secondary flow structure and the associated thermal characteristics in a mixed convective flow through a bottom heated horizontal rectangular duct can be significantly affected by the duct aspect ratio  $A$  (duct width/duct height), in addition to the Prandtl, Reynolds and Rayleigh numbers. In a low aspect ratio duct ( $A \leq 4$ ) the viscous damping effects of the side walls are expected to play an important role in determining the vortex flow characteristics under certain situations specified by the Prandtl, Reynolds and Rayleigh numbers. While in a high aspect ratio duct ( $A \geq 10$ ) the vortex flow has more space to move in the spanwise direction and can be rather complex. However, the details on how the aspect ratio affects the vortex flow remain largely unexplored. The understanding of this aspect ratio effect is relatively important in improving the growth of the single crystal film from the chemical vapor deposition processes. In the present study combined flow visualization and temperature measurement were carried out to investigate the effects of the aspect ratio on the spatial and temporal structures of the vortex flow induced in a

mixed convection of air in a bottom heated rectangular duct. Attention was focused on the change of the longitudinal vortex flow structure with the aspect ratio for various Reynolds and Rayleigh numbers.

Considerable research has been carried out to explore various characteristics of the buoyancy induced longitudinal vortex rolls in the mixed convective flow through a bottom heated rectangular duct from the stability analysis [1–4], experimental measurement [5–9] and numerical simulation [10–13] over wide ranges of the Reynolds and Rayleigh numbers covering the steady and time-dependent mixed convection for high and low aspect ratios. Nevertheless, very few results were obtained for the duct with an intermediate aspect ratio for  $A = 5–7$ . Moreover, no result was reported in the literature when  $A$  is an odd number. A detailed review of the literature on the longitudinal vortex flow was given in our previous study [13].

Much less works were conducted for the transverse vortex flow at an extremely low Reynolds number. The existence of the transverse thermoconvective rolls was experimentally proved by Luijckx and Platten [14] in a mixed convection of silicone oil ( $Pr \approx 450$ ) in a high aspect ratio rectangular duct. The critical Rayleigh number for the onset of the transverse rolls was found to be a function of the aspect ratio, Reynolds

† Author to whom correspondence should be addressed.

### NOMENCLATURE

$A$	aspect ratio, $b/d$	$t_p$	oscillation period [s]
$b$	channel width	$W$	axial velocity
$d$	channel height	$x, y, z$	dimensionless Cartesian coordinates, scaled with $d$ .
$Gr$	Grashof number, $g\beta d^3(T_h - T_c)/\nu^2$		
$F$	dimensionless frequency, $f/(\alpha/d^2)$		
$f$	frequency [Hz]		
$g$	gravitational acceleration	Greek symbols	
$Nr$	number of the longitudinal rolls	$\alpha$	thermal diffusivity
$Ra$	Rayleigh number $g\beta d^3(T_h - T_c)/\nu\alpha$	$\beta$	thermal expansion coefficient
$Re$	Reynolds number $W_m d/\nu$	$\nu$	kinematic viscosity.
$T$	temperature	Subscript	
$T_c, T_h$	top and bottom plate temperatures	$m$	average value.
$t$	dimensional time		

and Prandtl numbers. A flow regime map for nitrogen gas was proposed by Chiu *et al.* [15, 16] to locate the boundaries among the flow with no rolls, steady and unsteady vortex rolls. Ouazzani *et al.* [17, 18] provided a relation between the wave speed, mean velocity and Rayleigh number for air flow with  $1 \leq Re \leq 9$  and  $12,000 \leq Ra \leq 20,000$ . They also refined the flow regime map to include the transverse rolls. The effects of the inlet and exit boundary conditions on the characteristics of the transverse vortex flow at a slightly supercritical Rayleigh number were explored through solving the one-dimensional amplitude equations and two-dimensional Navier–Stokes equations by Müller *et al.* [19].

The above literature review reveals that no systematic study on how the vortex flow characteristics in a bottom heated rectangular duct are influenced by the duct aspect ratio was conducted in the past. An experiment including flow visualization and temperature measurement was carried out in this study to unravel the relation between the vortex flow structure and aspect ratio in mixed convection of air in a bottom heated rectangular duct. In the experiment the aspect ratio was varied from 2 to 12, the Reynolds number from 2.5 to 50 and the Rayleigh number from 3000 to 20,000, covering the steady and time-dependent flow. Both the changes in the spatial and temporal structures will be examined in detail.

## 2. EXPERIMENTAL APPARATUS AND PROCEDURES

### 2.1. Experimental apparatus

A sketch of the established test apparatus for the mixed convection of air in a bottom heated horizontal plane channel and the adopted coordinate system are shown in Fig. 1. The test section is a rectangular duct of 240 mm wide and 300 mm long with the gap width of 20 mm between the hot and cold walls. Thus the aspect ratio of the duct is 12. Adjustment of the aspect

ratio will be discussed later. The lower plate of the test section is made of a 15 mm thick, high purity copper plate and is electrically heated by d.c. power supplies. The heaters glued onto the outside surface of the bottom wall were divided into 10 segments in the flow direction and each heater was independently controlled by a GW GPC 3030D laboratory power supply. The width of the lower plate is 40 mm larger than that of the test section in order to reduce the edge effect of the test section. The upper plate of the test section is made of 3 mm thick glass plate. The plate is reinforced by a copper alloy frame to keep it flat. The upper plate is cooled by distilled water flowing above it. The distilled water is maintained at a constant temperature by a constant temperature circulator which consists of a heater, a cooler and a 90,000 gallon underground water reservoir. This circulator can control the temperature of the distilled water within  $\pm 0.1^\circ\text{C}$ . The volume flow rate of the distilled cooling water is adjusted carefully so that the temperature difference in the cooling water over the glass plate is within  $\pm 0.1^\circ\text{C}$ . The water head is also suitably adjusted to minimize any possible deformation in the glass. The side walls of the test section are made of 5 mm thick plexiglass.

The temperature of the lower plate is measured by 13 calibrated and electrically insulated T-type thermocouples embedded in the plate. The temperature of the upper plate is measured by six T-type thermocouples stuck to the inside surface of the plate. The temperatures of both plates could be maintained at nearly uniform and constant values with the deviations ranging from  $\pm 0.05$  to  $\pm 0.12^\circ\text{C}$ . For each experiment the top plate temperature is kept at the same value as that of the inlet air flow for the purpose of eliminating the formation of a thermal boundary layer on the top wall.

The open loop mixed convection apparatus begins with the air regulated from a 600 psi and 50,000 cubic feet high pressure air tank which is passed through a

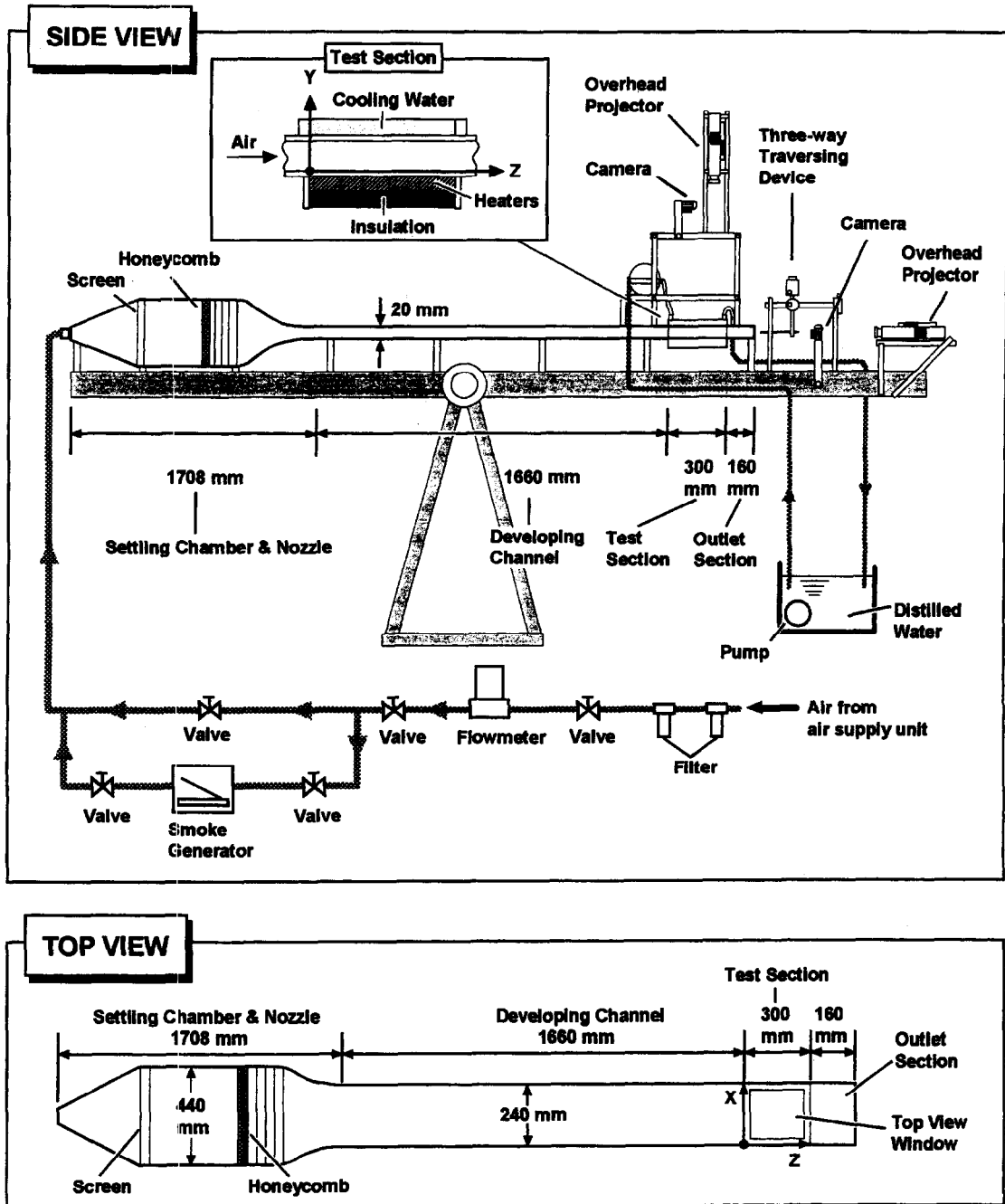


Fig. 1. Schematic of test apparatus and the chosen coordinate system.

settling chamber, a contraction nozzle and a developing channel before entering into the test section. In the settling chamber turbulence is suppressed by first passing the air through two fine mesh screens, then a honeycomb section and finally four fine mesh screens. The nozzle with a contraction ratio of 20:1 has been designed to eliminate flow separation, minimize turbulence and provide a nearly uniform velocity at the inlet of the developing section. The developing section is 1660 mm in length, approximately 83 times the

channel height. This insures the flow being fully developed at the inlet of the test section for  $Re \leq 50$ . After the test section, a 160 mm outlet section is added to reduce the disturbance resulting from discharging the flow to the ambient. The settling chamber and the contraction nozzle are made of stainless steel, whereas the developing channel and the outlet section are made of 5 mm thick plexiglass. The whole test apparatus is placed in a quiescent house to eliminate any possible disturbance from the ambient outside the house. The

entire loop is insulated with the superlon insulator of 20 mm thick and is mounted on a rigid supporting frame.

The volume flow rate of air is controlled and measured by a Hasting HFC flow controller with an accuracy better than 1%. The flow measuring system is calibrated periodically by a Brooks bell prover with an accuracy of 0.2%. The operating condition of the flowmeter in actual measurement is adjusted to a condition similar to that of the calibration stand. The mean air speed in the test section is calculated from the total flow rate.

To measure the velocity and temperature distributions in the flow, probes are inserted from the downstream end of the test section. The probes are supported by a three-way traversing device. Velocity is measured by a hot-wire probe. For calibrating the hot-wire, the pipe flow method that the probe is placed in the center of a fully-developed laminar pipe flow is used. The total flow rate is measured and the pipe center velocity is calculated from the parabolic distribution. The temperature is measured by a thermocouple probe which is an OMEGA (model HYPO) mini hypodermic extremely small T-type thermocouple (33 gauge) implanted in a 1 in long stainless steel hypodermic needle.

## 2.2. Data uncertainty

The data acquisition and control system and various instruments, including a PC 486-66, multiplexers (Computer Products RTP 743 series), a digital barometer (Setra Systems 361B), reference junctions (Celesco Transducer Products BRJ 14), laboratory power supplies (GW GPC 3030D), OMEGA type T thermocouples, a Hasting HFC flow controller and a data reduction software are calibrated and adjusted end to end on site by Instrument Calibration Section, Q.A. Center, Chung Shan Institute of Science and Technology (CSIST), Taiwan with the transfer standards that the calibration hierarchy can trace back to the standards of the National Institute of Standard and Technology (NIST), U.S.A. Before performing the end to end calibration all the sensors and transducers used were transported to CSIST for calibration or adjustment with the inter-lab standards based on the test point that will be encountered in the present test to get best calibration curve fit data. The main purpose of this calibration is to reduce any possible bias between the true physical value and the readout of the sensors and transducers. The data reduction error is reduced further by using the best nonlinear least-square calibration curve fits and by selecting a suitable gain code of the multiplexers. The system is well grounded and the electric noises are suitably filtered out. Fixed physical or simulated signals are then applied in the data uncertainty test. Samples higher than 32 are measured at each test point during the data uncertainty test. Uncertainties in the Rayleigh number, Reynolds number and other independent parameters were calculated according to the standard

procedures established by Kline and McClintock [20] and Abernethy and Thompson [21]. The uncertainties due to the control unsteadiness and temperature non-uniformity are also accounted for in the data uncertainty evaluation. In addition, the uncertainties of the thermal physical properties of the air were also included in the analysis. The fundamental thermophysical properties of the working fluids are  $\alpha = 0.220$  ( $\text{cm}^2 \text{s}^{-1}$ ),  $\beta = 0.00335$  ( $\text{K}^{-1}$ ),  $Pr = 0.737$  and  $\nu = 0.162$  ( $\text{cm}^2 \text{s}^{-1}$ ) at  $30^\circ\text{C}$  and 0.997 bar. The fluid properties are real time corrected based on the temperature and pressure detected in the test section inlet.

The detailed uncertainty analysis indicated that the uncertainties of temperature, volume flowrate, dimension, Reynolds number and Rayleigh number measurements are estimated to be  $\pm 0.15^\circ\text{C}$ ,  $\pm 5\%$ ,  $\pm 0.05$  mm,  $\pm 6\%$  and  $\pm 6\%$ , respectively.

## 2.3. Adjustment of the side walls

The aspect ratio of the test section can be reduced by inserting two additional, extended side walls of 12.5 mm thick into the duct. The additional side walls extend from the exit of the settling chamber through the developing and test sections and end at the duct exit. Besides, the additional side walls have sharp leading and trailing edges to minimize their disturbances to the flow. Moreover, four scaled windows were, respectively, located at the exit of the settling chamber, inlet of the test section, outlet of the test section and exit of the loop to monitor the proper position of the side walls during the test.

## 2.4. Preliminary investigation of flow field

At first, the main forced flow is investigated to check its fully developed condition at the entrance of the test section with no heat input to the bottom plate. Figure 2 shows the sampled data from the hot wire measure-

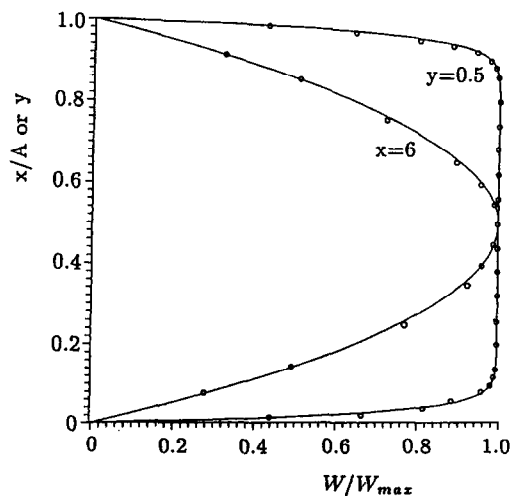


Fig. 2. Comparison of the measured axial velocity profiles  $w/w_{\max}$  at the inlet with the analytical solution from Shah and London [22]; circles: experimental data and solid curves: analytic solution.

ment for a typical case with  $Re = 50$  and  $A = 12$ . The results clearly indicate that at the test section inlet the velocity profile is fully developed and is in good agreement with the analytical results given by Shah and London [22]. Additionally, the turbulence intensity is found to be less than 0.7%.

Flow visualization was conducted to observe the secondary flow patterns from the top, side and end views by injecting smoke at some distance ahead of the settling chamber. They were carried out by using a 1.5–2.5 mm plane light beam to shine through the flow field containing tiny incense particles as the light scattering centers and a sharp contrast could be achieved between the duct walls and the smoke.

In all the experiments to be reported below, we first adjust the additional side walls to the required aspect ratio. Next, we imposed a fully developed flow in the entire test section and then turned on the power supply to the bottom plate and in the mean time circulated the chilled water over the top plate. It took about 3 h for the Rayleigh number  $Ra$  to raise to the test point and required about another 2 h for  $Ra$  to stabilize. After this we began various measurements and flow visualization.

### 3. RESULTS AND DISCUSSION

In the ranges of the parameters covered in this study the buoyancy induced vortex flow is mainly in the form of regular and deformed longitudinal rolls. Thus in the following selected results from the top and end views of the vortex flow and the time histories of the air temperature are to be presented to illustrate the spatial structures of the flow and the associated temporal structures in ducts of various aspect ratios for different Reynolds and Rayleigh numbers.

#### 3.1. Spatial structure of vortex flow

Results are first presented in Fig. 3 to demonstrate the effects of the aspect ratio on the steady longitudinal vortex flow at a low buoyancy-to-inertia ratio for typical cases with  $Re = 40$  and  $Ra = 6000$ . The top view flow photos at steady-state indicate that in a duct with a large aspect ratio for  $A = 12$  three rolls are successively induced near each side wall [Fig. 3(a)]. The onset point of the roll is closer to the duct inlet when the roll is closer to the side wall. The cross-section of each roll gradually grows with the downstream distance. At the duct exit the roll size is approximately equal to the duct height. Outside the rolls the flow is unidirectional and is forced convection dominated. Besides, the flow is in spanwise symmetry. It is noted that at a lower aspect ratio for  $A = 8$  the induced longitudinal rolls near the duct sides [Fig. 3(b)] resemble those for  $A = 12$  given in Fig. 3(a), but the spanwise extent of the forced convection dominated region is substantially reduced at  $A = 8$ . Detailed comparison reveals that at this low buoyancy-to-inertia ratio a reduction of the aspect ratio from 12 to 8 is equivalent to take the central portion

of the wide duct around the vertical central plane at  $x = A/2$  away, so that  $A$  is reduced to 8 as far as the induced vortex flow is concerned. A similar effect is noted when  $A$  is further reduced to 6. At  $A = 6$  the roll number is equal to the aspect ratio and the rolls in the exit region of the duct are in close contact with each other and no forced convection dominated region exists in the duct exit [Fig. 3(c)]. Note that at a still lower aspect ratio of  $A = 4$  the induced vortex rolls [Fig. 3(d)] are equivalent to take the two rolls near the central vertical plane at  $x = A/2$  away from the duct with  $A = 6$ . For an even smaller aspect ratio of  $A = 3$  only two rolls are induced near the duct sides [Fig. 3(e)]. At  $A = 2$  we also have two rolls in the duct [Fig. 3(f)]. For these cases the resulting flow is steady and spanwisely symmetric. A close inspection of these results, however, indicates that the onset points of the corresponding rolls for various  $A$  are slightly different.

Next, how the unsteady asymmetric longitudinal vortex flow for a higher  $Gr/Re^2$  is affected by the aspect ratio is examined. Snapshots of the flows from the top view for typical cases at a high buoyancy-to-inertia ratio with  $Re = 50$  and  $Ra = 20,000$  are shown in Fig. 4 for various aspect ratios. For  $A = 12$  the flow is in a large amplitude irregular oscillation and is asymmetric [9]. These flow photos also suggest that at a reducing aspect ratio the resulting vortex flow is approximately the same as that in a wider duct with the vortex flow in the duct core taken away. Inspecting the detailed vortex flow characteristics, however, discloses that when the aspect ratio is decreased from 12 to 8 the unsteady flow becomes less irregular and asymmetric. For  $A \leq 6$  the induced flow evolves to a steady and symmetric state. Additionally, it is noted that at  $A = 3$ , four vortex rolls prevail in the duct with the two rolls in the duct core being much smaller than those near the side walls. This decrease of the roll size toward the duct core is often seen when  $A$  is an odd number.

Effects of the Reynolds number on the vortex flow in ducts of different aspect ratios are then investigated. Figure 5 shows the instantaneous top view flow photos for  $Re = 30$ – $50$  at  $A = 4$  and 12 for  $Ra = 20,000$ . The results manifest that in the high aspect ratio duct ( $A = 12$ ) a lowering of the Reynolds number causes the unsteady flow to become more irregular with more frequent splitting and merging of the longitudinal rolls, in addition to the movement of the onset point to the more upstream region [9], but in the low aspect ratio duct ( $A = 4$ ) the flow remains steady for the Reynolds number reduced from 50 to 40 and then to 30, although the onset of the rolls still moves upstream. Nevertheless, significant change in the cross-section of the longitudinal rolls with the Reynolds number is noted. At  $Re = 40$  and 30 the roll cross-sections deviate substantially from the circular shape, which is normally observed in the steady longitudinal vortex flows as in Fig. 3. To further illustrate the vortex flow change with the Reynolds number in a low aspect ratio duct, Fig. 6 presents a series of the

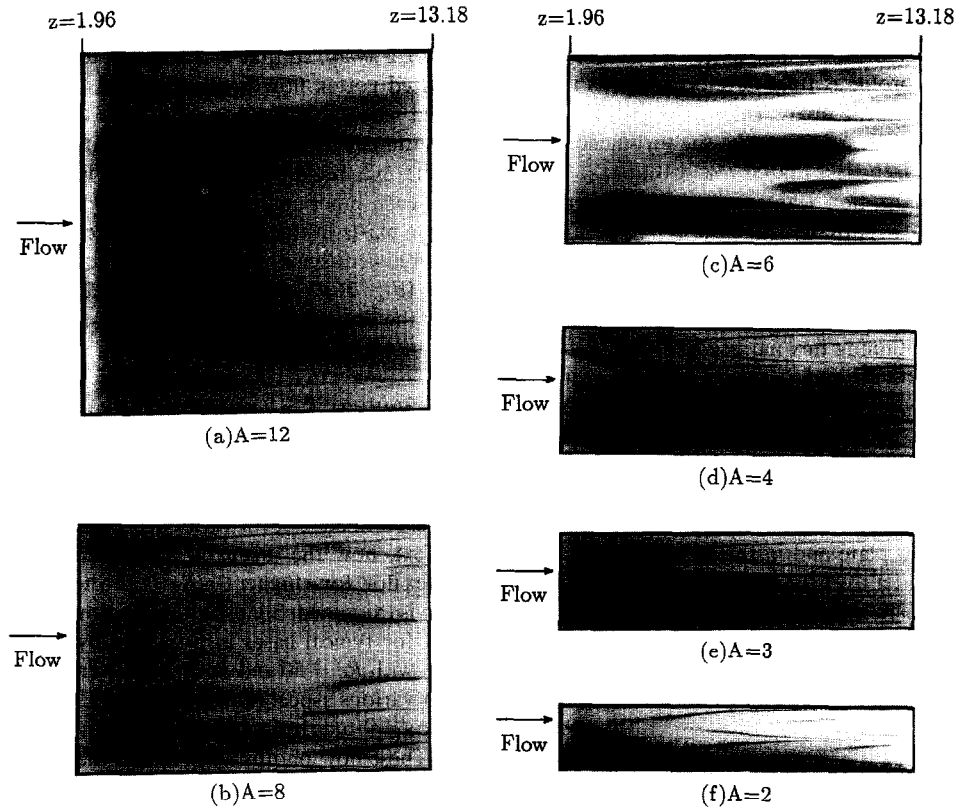


Fig. 3. Top view of the vortex flow at  $y = 0.5$  at  $Re = 40$  and  $Ra = 6000$  for: (a)  $A = 12$ ; (b)  $A = 8$ ; (c)  $A = 6$ ; (d)  $A = 4$ ; (e)  $A = 3$ ; and (f)  $A = 2$ .

instantaneous top view flow photos for  $Re$  reduced from 50 to 5 for  $A = 4$  and  $Ra = 6000$ . The results suggest that for  $15 \leq Re \leq 50$  reducing the Reynolds number simply causes the four steady longitudinal rolls to be induced at a shorter distance from the duct inlet and the vortex flow to become stronger [Figs 6(a)–(c)]. When  $Re$  is further lowered to 10, the buoyancy-to-inertia ratio ( $Gr/Re^2$ ) is so high that the resulting flow [Fig. 6(d)] evolves to a time periodic state in the downstream portion of the duct. This will be discussed later. The two rolls in the duct core exhibit some deformation in the roll cross-section, but the rolls near the duct sides are still in a regular shape. This interesting flow pattern is also observed for a slightly lower  $Re$  of 7.5. Figures 6(e) and (f) show that at  $Re = 7.5$  there are cyclic expansion and contraction of the roll cross-sections with time for the downstream portion of the two rolls in the duct core. It is worth mentioning that the time periodic flows driven at  $Re = 10$  and 7.5 are still in spanwise symmetry. At an even lower Reynolds number of 5, snaking vortex rolls with significant variations in the roll cross-section in the entry half of the duct are noted [Figs 6(g) and (h)]. Slightly downstream roll merging takes place. Near the duct exit the flow becomes rather irregular and is somewhat asymmetric. Moreover, a large change in the flow pattern with time appears in the exit portion of the duct.

The detailed structural change in a snaking vortex flow induced at a high buoyancy-to-inertia ratio for  $Re = 5$  and  $Ra = 5000$  with  $A = 4$  is illustrated in Fig. 7 for a typical periodic cycle ( $t_p = 20$  s). It is noted from the top view photos that near the duct exit the vortex rolls significantly swing with time in the spanwise direction. In this snaking flow the rolls in the duct core near the duct exit grow in the first half of the period and decay in the other half of the period with the accompanied decay and growth of the other rolls near the duct sides, as evident from the end view flow photos [Fig. 7(b)]. To further investigate the axial development of the complex vortex flow containing the roll snaking, merging and splitting, Fig. 8 gives the snapshots of the flow from the top and end views at selected time instants in a periodic cycle at selected cross-sections for an even higher buoyancy-to-inertia ratio with  $Re = 5$  and  $Ra = 6000$  for  $A = 4$ . The results suggest that in the entry region of the duct the vortex flow is steady and consists of four regular longitudinal rolls of nearly equal size. Slightly downstream the rolls become snaking with the cyclic expansion and contraction of the roll cross-sections in time. The roll expansion and contraction get increasingly significant as the flow moves downstream. Beyond certain axial stations the four rolls in a period are found to merge into two rolls at first, split into four rolls later, and then further split into six rolls, as

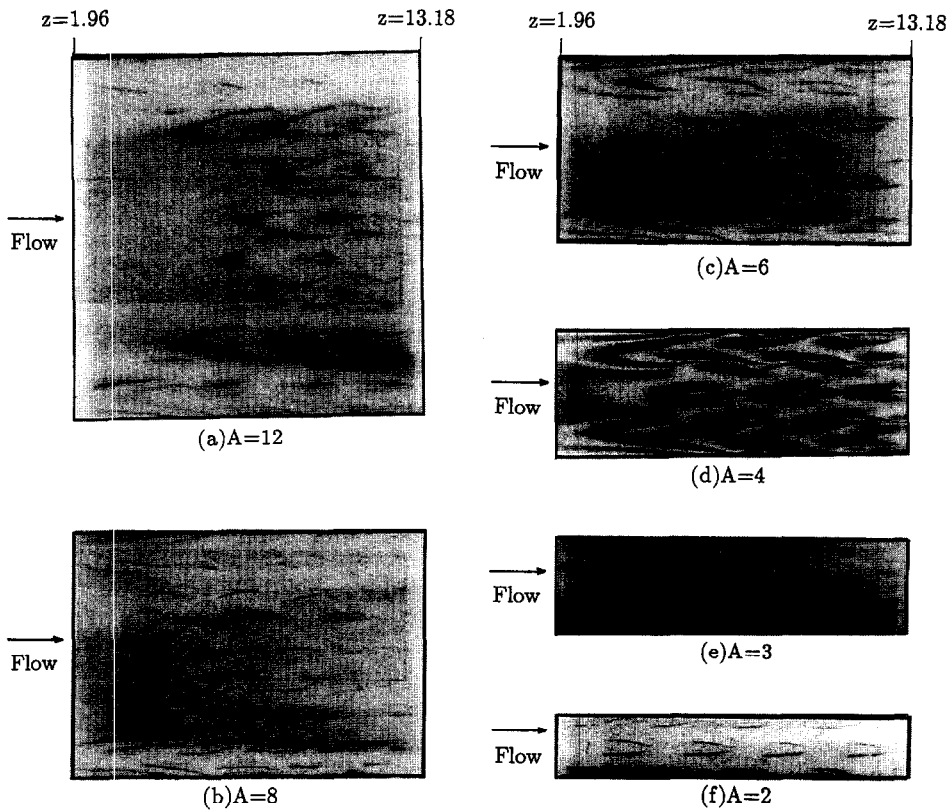


Fig. 4. Top view of the vortex flow at  $y = 0.5$  at  $Re = 50$  and  $Ra = 20,000$  for: (a)  $A = 12$ ; (b)  $A = 8$ ; (c)  $A = 6$ ; (d)  $A = 4$ ; (e)  $A = 3$ ; and (f)  $A = 2$ .

indicated by the results for  $z = 10.94$  in Fig. 8(b). This roll merging and splitting processes repeat periodically in time with  $t_p = 20$  s. In the exit portion of the duct the vortex flow is mainly dominated by the two large longitudinal rolls in addition to the frequent appearance of a small, weak roll near each side wall. The flow is no longer in spanwise symmetry in this portion of the duct. Note that the space prevailed by the snaking rolls changes significantly with time.

Some interesting vortex flow patterns induced in a duct with its aspect ratio being an odd number are shown in Fig. 9 for  $A = 3$  and 5. Depending on the particular set of the governing parameters investigated, the vortex flow for  $A = 3$  can be in the form of two steady symmetric longitudinal rolls with  $Re = 30$  and  $Ra = 5000$ , four steady symmetric rolls of unequal size at  $Re = 40$  and  $Ra = 8000$ , or two unsteady, deformed, but spanwisely symmetric rolls in the duct core with no rolls induced near the duct sides at  $Re = 7.5$  and  $Ra = 4000$ . While for  $A = 5$  the duct can be filled with six steady symmetric rolls of unequal size for  $Re = 30$  and  $Ra = 5000$ , and  $Re = 40$  and  $Ra = 8000$ , or two unsteady symmetric rolls in the region between the duct sides and axis for  $Re = 5$  and  $Ra = 3000$ .

It is of interest to point out that for the steady longitudinal vortex flow the maximum number of rolls  $Nr$  induced in the duct is always even for both odd

and even aspect ratios. A simple rule for  $Nr$  deduced from the present data can be summarized as

$$Nr = A \text{ for even } A \quad (1)$$

$$Nr = A + 1 \text{ for odd } A \text{ with } A \geq 5 \quad (2)$$

$$Nr = A - 1 \text{ for } A = 3 \text{ with low } Re \text{ and } Gr/Re^2 \quad (3)$$

$$Nr = A + 1 \text{ for } A = 3 \text{ with high } Re \text{ and } Gr/Re^2. \quad (4)$$

Thus, the roll size can be less than, equal to or greater than the channel height.

### 3.2. Temporal structure of vortex flow

In our previous experimental investigation [9] of the buoyancy driven vortex air flow in a high aspect ratio rectangular duct ( $A = 12$ ) the transition from steady to time-dependent states was found to be subcritical at increasing Rayleigh or decreasing Reynolds number. This subcritical transition is characterized by a sudden change from steady to chaotic states and no time periodic state was detected in the experiment. In a lower aspect ratio duct the present data clearly show the presence of time periodic states during the flow transition over certain ranges of  $Re$  and  $Ra$ . In the following the temporal characteristics of the flow are illustrated by showing the time variations of the instantaneous air temperature at statistical state at selected locations for various cases.

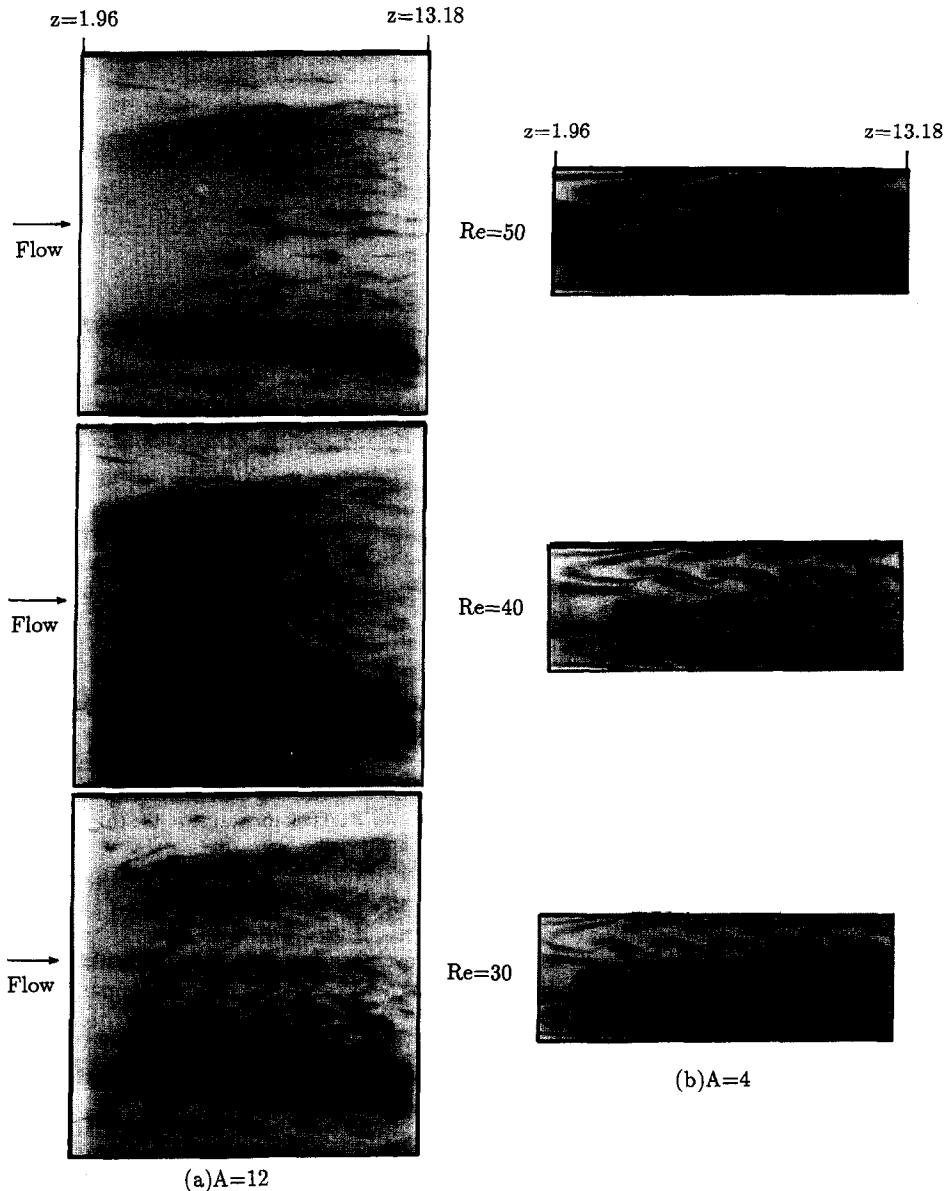


Fig. 5. Top view of the vortex flow at  $y = 0.5$  for various Reynolds numbers at  $Ra = 20,000$  for: (a)  $A = 12$  (unsteady flow); and (b)  $A = 4$  (steady flow).

First, the time records of the air temperature associated with the cyclic expansion and contraction of the roll cross-section in the downstream portion of a low aspect ratio duct at various axial stations are given in Fig. 10 for an exemplified case with  $Re = 10$ ,  $Ra = 7000$  and  $A = 4$  along with the corresponding spatial structures. The results indicate that in the entry half of the duct the flow is steady and the rolls do not change their sizes with time. Slightly downstream the flow starts to exhibit a small amplitude intermittent oscillation, as evident from the results for  $z = 9.26$  in Fig. 10(b). In the exit portion of the duct the flow evolves to a time periodic state except in the narrow region near the central vertical plane at  $x = A/2$  where

the flow is still intermittent. The period of the oscillation is 11.9 s. Note that the amplitude of the oscillation grows gradually with the downstream distance.

In the snaking longitudinal vortex rolls induced at a higher buoyancy-to-inertia ratio (Fig. 7), the amplitude of the flow oscillation shown in Fig. 11 for  $Re = 5$  and  $Ra = 5000$  is larger especially in the downstream region between the duct core and side walls where the roll snaking is intense. At this low  $Re$  the period of the oscillation is longer with  $t_p = 20$  s.

At an even higher buoyancy-to-inertia ratio the vortex flow contains significant roll snaking in the entry half of the duct, roll merging and splitting slightly downstream, and irregular asymmetric rolls near the



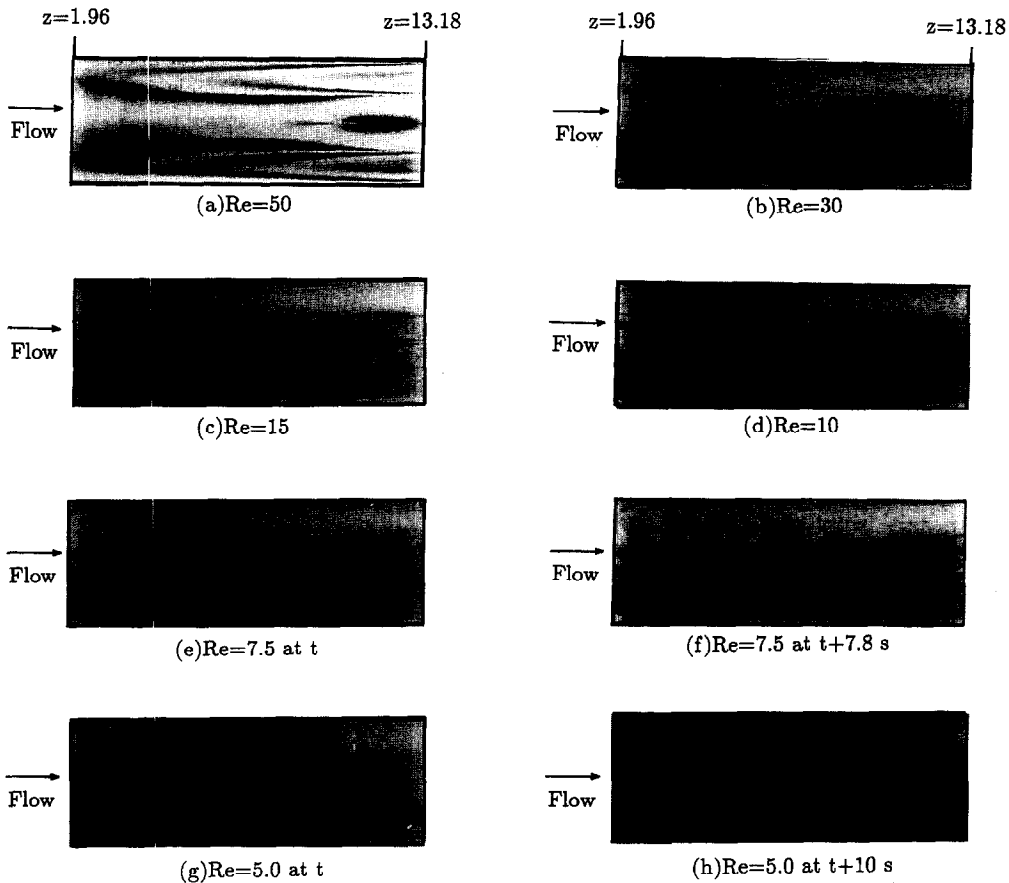


Fig. 6. Effect of reducing Reynolds number on the vortex flow patterns for  $A = 4$ ,  $Ra = 6000$  and (a)  $Re = 50$ ; (b)  $Re = 30$ ; (c)  $Re = 15$ ; (d)  $Re = 10$ ; (e)–(f)  $Re = 7.5$ ; and (g)–(h)  $Re = 5.0$  ( $t$  denotes a certain time instant in a statistical state).

duct exit, as discussed above in Fig. 8. The corresponding temporal flow characteristics given in Fig. 12 for a typical case with  $Re = 5$ ,  $Ra = 6000$  and  $A = 4$  suggest that the flow is time periodic in the region dominated by the snaking rolls ( $t_p = 20$  s) in the duct entry. As the roll merging and splitting prevail, the flow shows some irregular oscillation and there is a significant axial increase in the oscillation amplitude in the duct core. The flow oscillation is relatively irregular in the asymmetric rolls near the duct exit.

The vortex flow oscillates at a much higher frequency when the Reynolds number is much higher, as evident from the data in Fig. 13 for  $Re = 20$ ,  $Ra = 20,000$  and  $A = 4$ . The oscillation period is 5.6 s in the middle portion of the duct. In this case the flow in the downstream half of the duct is characterized by the time oscillatory, twisted longitudinal rolls with significant roll expansion and contraction [Fig. 13(a)]. Note that in the entry half of the duct the flow is nearly steady. Downstream the flow becomes time periodic and there is a large increase in the oscillation amplitude with the downstream distance in the region close to the central vertical plane  $x = A/2$  and in the

region between the duct core and side walls. In this time periodic flow the spanwise symmetry is also preserved.

At an even lower aspect ratio ( $A = 2$ ) more significant roll snaking with a larger change in the roll cross sections with the space and time is induced, as evident by comparing the results in Fig. 14(a) with those in Fig. 11 for  $A = 4$  at the same Reynolds and Rayleigh numbers,  $Re = 5$  and  $Ra = 5000$ . Besides, at  $A = 2$  the snaking rolls are no longer in spanwise symmetry. Near the duct exit the flow is slightly irregular with no discernible spatial structure. The data for the corresponding time histories of the air temperature in Fig. 14(b) suggest that at  $A = 2$  the time periodic flow ( $t_p = 20$  s) is initiated at a shorter distance from the duct inlet and the oscillation amplitude is somewhat larger, when contrasted with those for  $A = 4$  in Fig. 11. Moreover, the temperature oscillation is not completely time periodic in the exit portion of the duct.

An examination of the data for the oscillation frequencies of the air temperature for a number of time periodic cases studied for various  $Re$  and  $Ra$  indicated that a reduction in the Reynolds number causes the

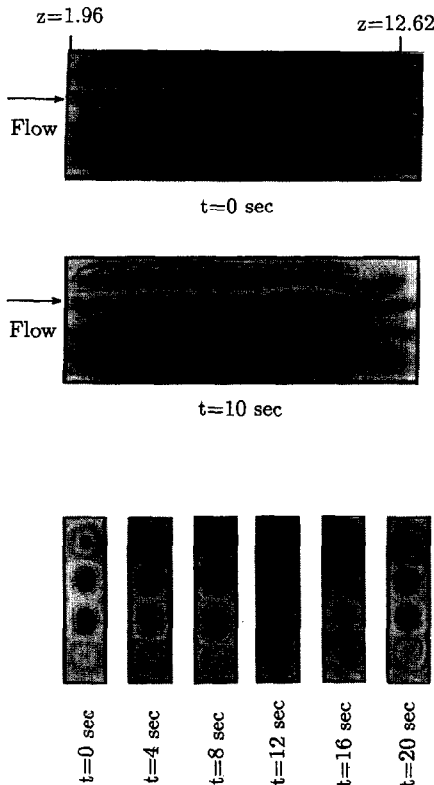


Fig. 7. Top and cross-sectional views of the vortex flow at selected time instants in a typical time period ( $t_p = 20$  s): (a) top view at  $y = 0.5$ ; and (b) end view at  $z = 12.62$  for  $A = 4$ ,  $Re = 5$  and  $Ra = 5000$ .

air temperature to oscillate in a lower frequency and the oscillation frequency is not affected by the Rayleigh number to any discernible degree. The data can be correlated as

$$f = 0.0088Re \tag{5}$$

or in dimensionless form

$$F = \frac{f}{(\alpha/d^2)} = 0.16Re \text{ for } 2.5 < Re \leq 20. \tag{6}$$

It was also noted that a raise in the Rayleigh number at a fixed Reynolds number only leads to a higher oscillation amplitude in the air temperature with little change in the oscillation frequency.

Finally, Fig. 15 gives the regime maps to delineate the boundaries between the steady regular vortex flow and time periodic snaking vortex flow for  $A = 2$  and 4 obtained herein. Note that the regimes for the existence of the periodic snaking rolls shift to a higher Rayleigh number as the Reynolds number is increased. Besides, the boundaries between the steady and time periodic flows, the so called 'Hopf bifurcation curves', can be correlated as:

$$Ra = 380Re + 2.8Re^3 \text{ for } A = 2 \tag{7}$$

$$Ra = 265Re + 2.4Re^3 \text{ for } A = 4. \tag{8}$$

A close scrutiny of the results reveals that the critical  $Ra$  for the Hopf bifurcation is slightly higher for  $A = 2$ .

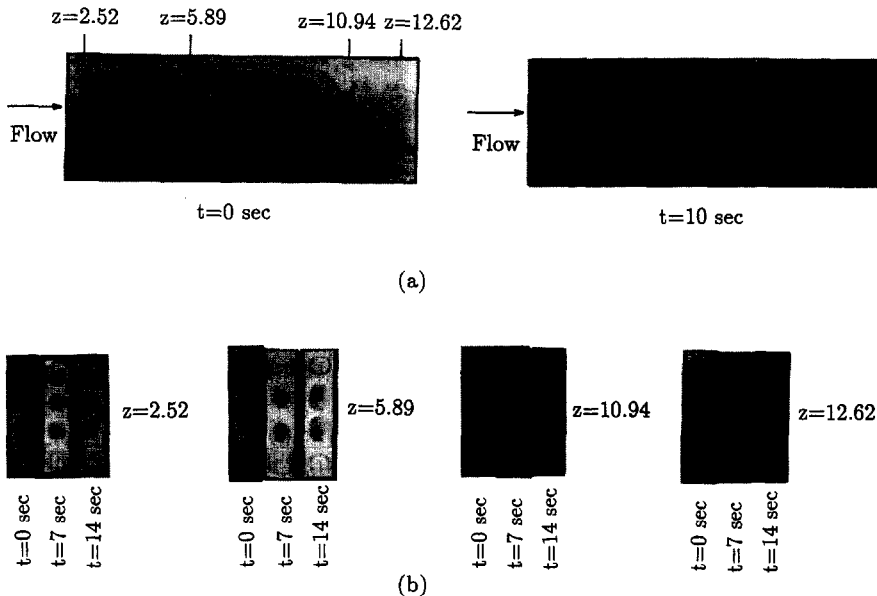


Fig. 8. Top and cross-sectional views of the vortex flow at selected time instants in a typical time period ( $t_p = 20$  s): (a) top view at  $y = 0.5$ ; and (b) end view at  $z = 2.52, 5.89, 10.94$  and  $12.62$  for  $A = 4$ ,  $Re = 5$  and  $Ra = 6000$ .

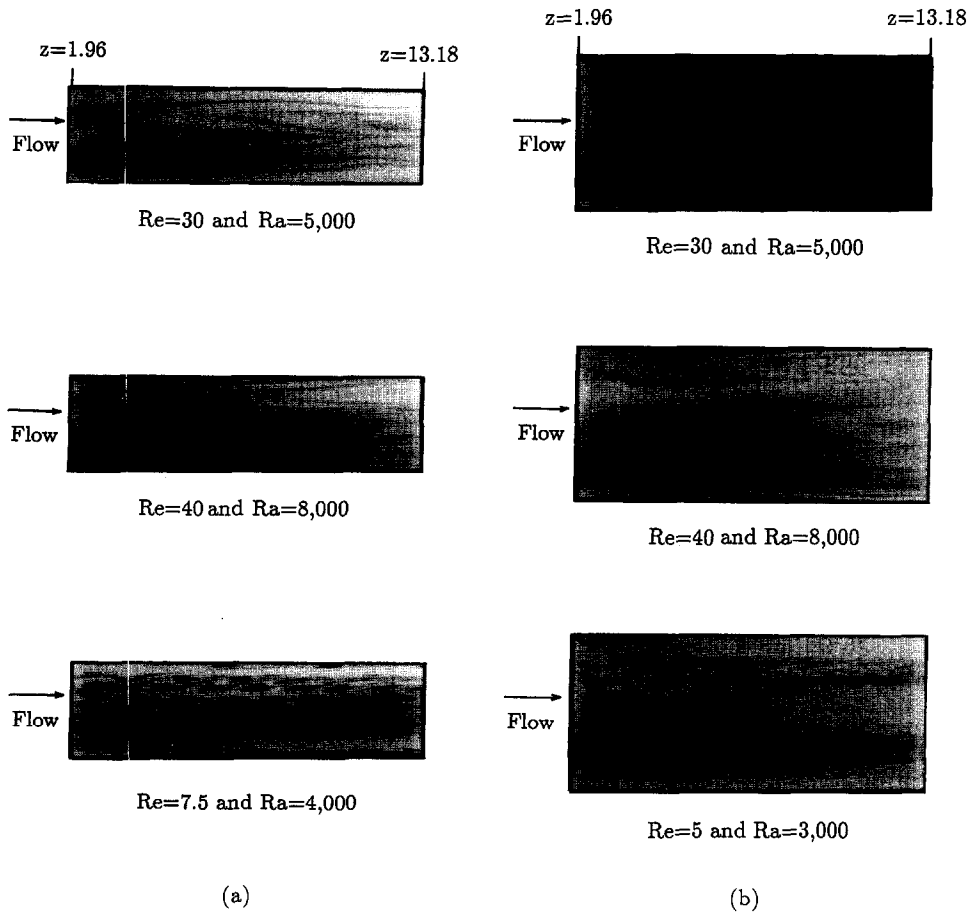


Fig. 9. Top view of the vortex flow at  $y = 0.5$  for various cases for: (a)  $A = 3$ ; and (b)  $A = 5$ .

#### 4. CONCLUDING REMARKS

In the present flow visualization and temperature measurement the effects of the aspect ratio on the steady and time-dependent longitudinal vortex flow in mixed convection of air in a bottom heated horizontal rectangular duct were investigated in detail. Major results obtained in this study can be summarized as follows:

(1) The main effect of reducing the aspect ratio on the spatial structures of the steady and unsteady longitudinal vortex flows is equivalent to remove the central portion of the duct. Besides, the unstable vortex flow at high  $Re$  and  $Ra$  can be stabilized when the aspect ratio is reduced.

(2) Reducing the Reynolds number in a high aspect ratio duct can cause the vortex flow to change from steady to unsteady state with more frequent roll splitting and merging. While in a low aspect ratio duct a reduction in the Reynolds number results in the distortion of the roll cross-section and can cause the vortex rolls to become snaking, accompanied with the cyclic roll expansion and contraction with time.

(3) When the value of the aspect ratio is an odd

number the number of the rolls induced in the duct is still even.

(4) At increasing buoyancy-to-inertia ratio the transition from a steady to a time-dependent state is subcritical when  $A$  is large, but in a lower aspect ratio duct there exists a finite range of the buoyancy-to-inertia ratio for the appearance of the time periodic snaking vortex flow with a spanwise symmetry. The corresponding oscillation frequency of the air temperature can be correlated as

$$F = \frac{f}{(\alpha/d^2)} = 0.16 Re. \quad (9)$$

It is important to emphasize that rich phenomena exist near the onset of convection which deserve special attention. Besides, the effects of aspect ratio on the transverse and mixed rolls and the effects of duct inclination are also important in various technological applications.

*Acknowledgement*—The financial support of this study by the engineering division of the National Science Council of Taiwan, Republic of China, through the contract NSC83-0404-E-009-054, is greatly appreciated.

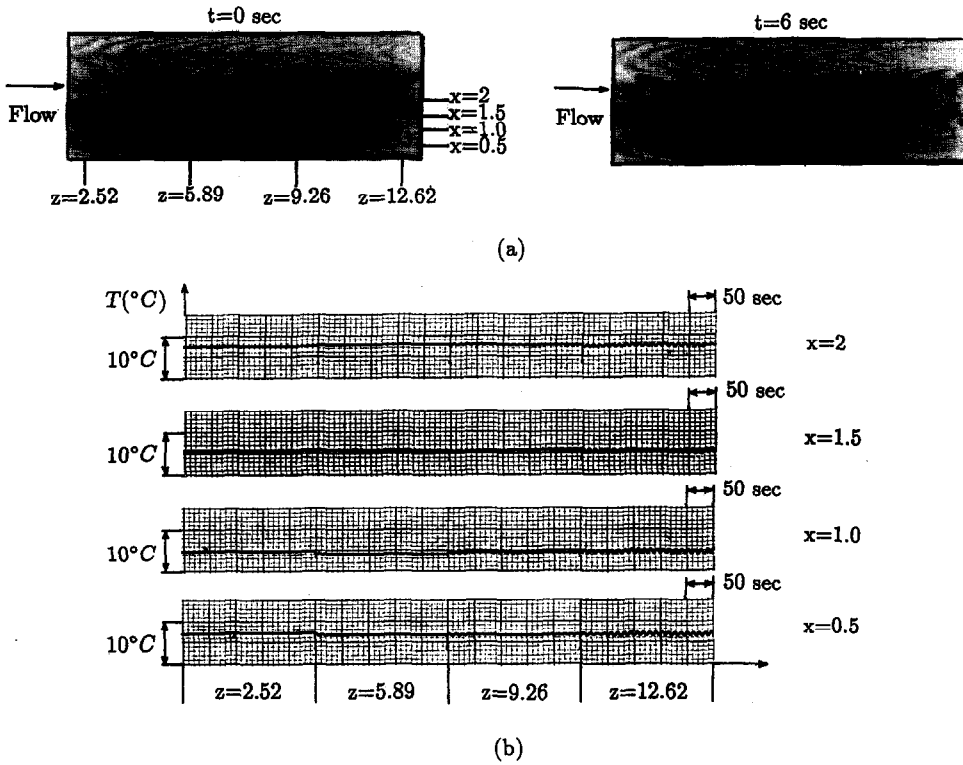


Fig. 10. Spatial-temporal structure of vortex flow: (a) top view photos at  $y = 0.5$ ; and (b) time records of air temperature at selected locations on lines  $y = 0.5$  and  $x = 2, 1.5, 1.0$  and  $0.5$  for  $A = 4$ ,  $Re = 10$  and  $Ra = 7000$  ( $t_p = 11.9$  s).

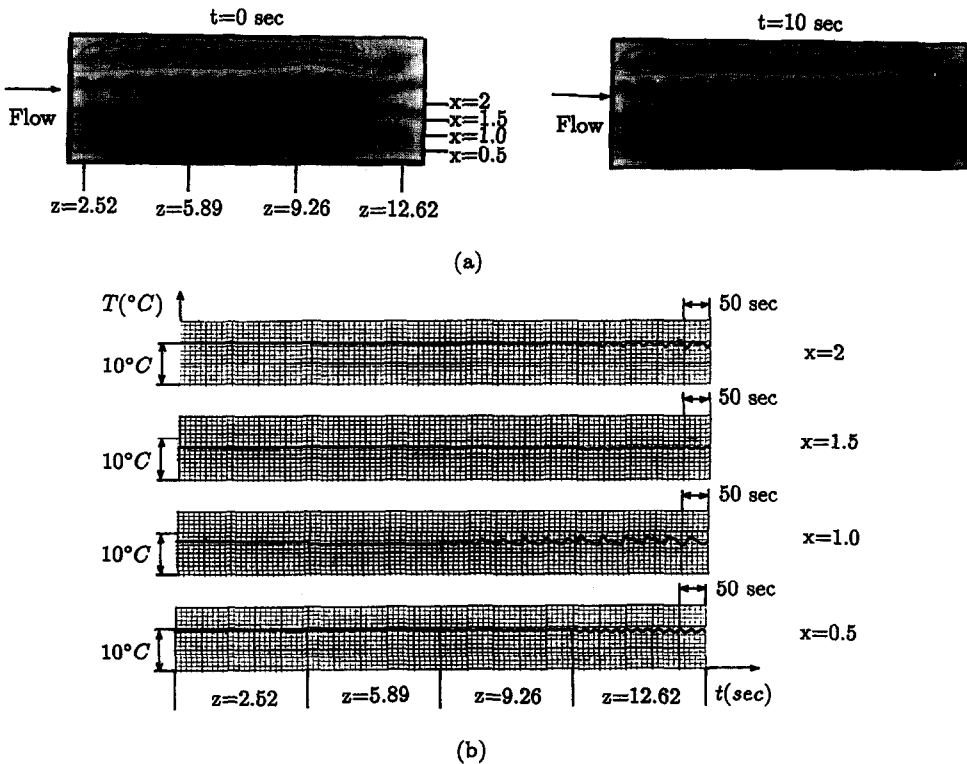


Fig. 11. Spatial-temporal structure of vortex flow: (a) top view photos at  $y = 0.5$ ; and (b) time records of air temperature at selected locations on lines  $y = 0.5$  and  $x = 2, 1.5, 1.0$  and  $0.5$  for  $A = 4$ ,  $Re = 5$  and  $Ra = 5000$  ( $t_p = 20$  s based on the data at  $x = 0.5$  and  $z = 12.62$ ).

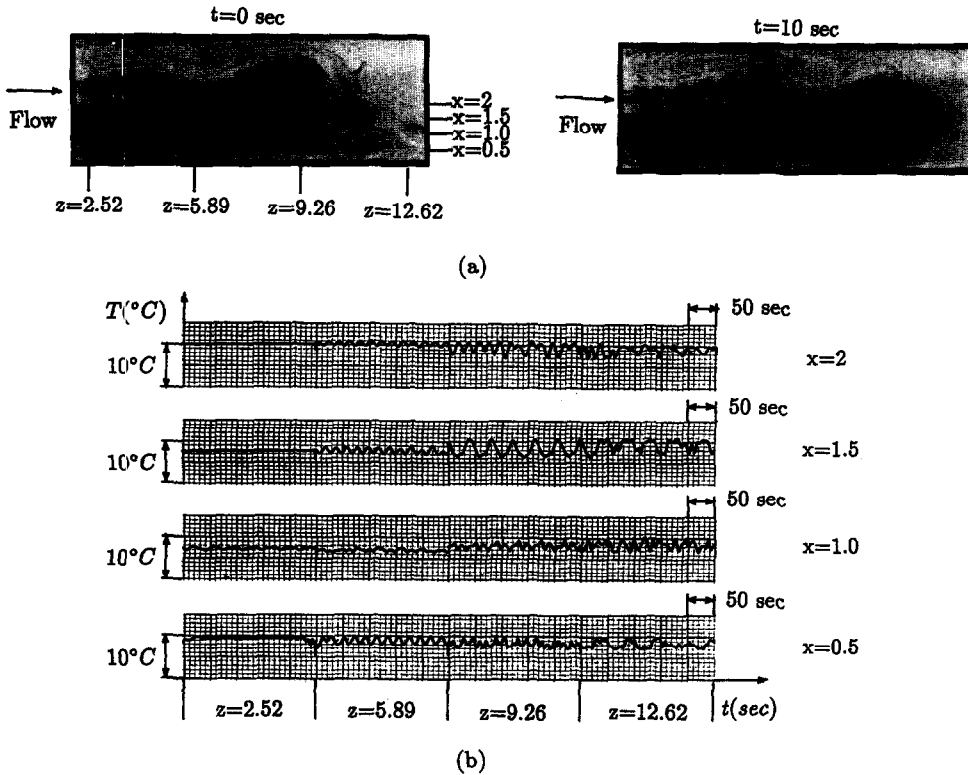


Fig. 12. Spatial-temporal structure of vortex flow: (a) top view photos at  $y = 0.5$ ; and (b) time records of air temperature at selected locations on lines  $y = 0.5$  and  $x = 2, 1.5, 1.0$  and  $0.5$  for  $A = 4$ ,  $Re = 5$  and  $Ra = 6000$  ( $t_p = 20$  s based on the data at  $x = 0.5$  and  $z = 5.89$ ).

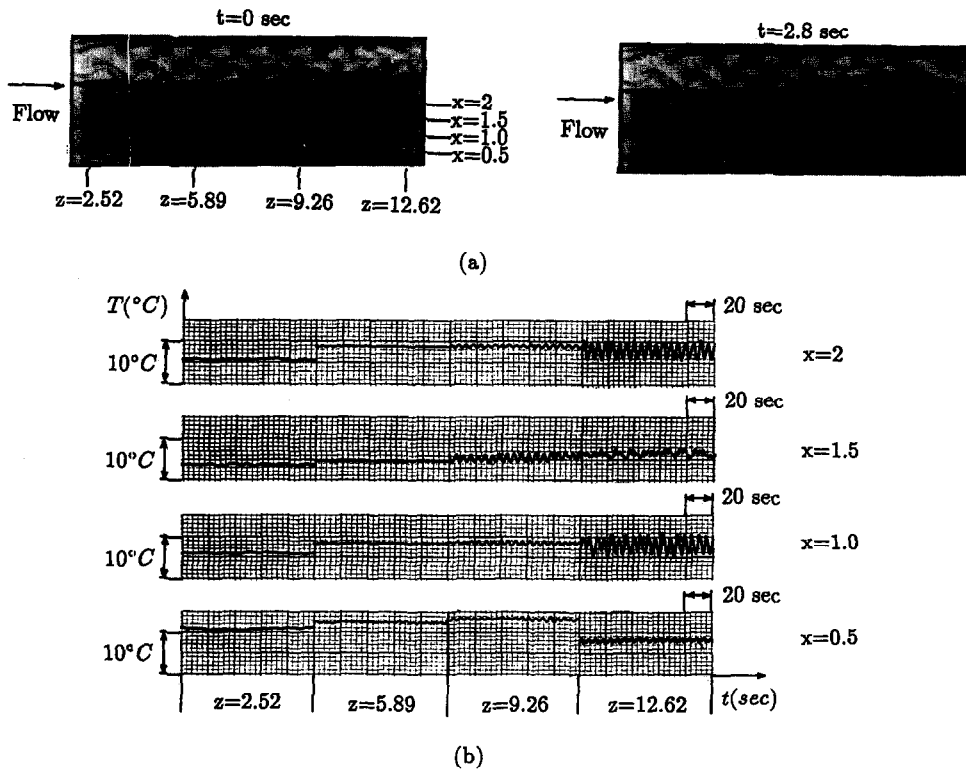
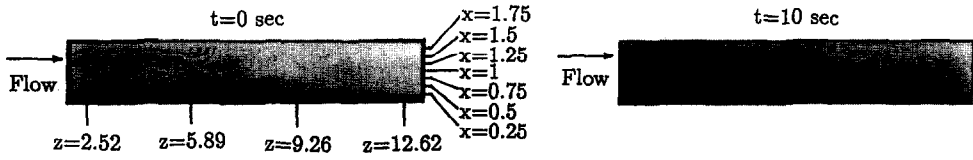
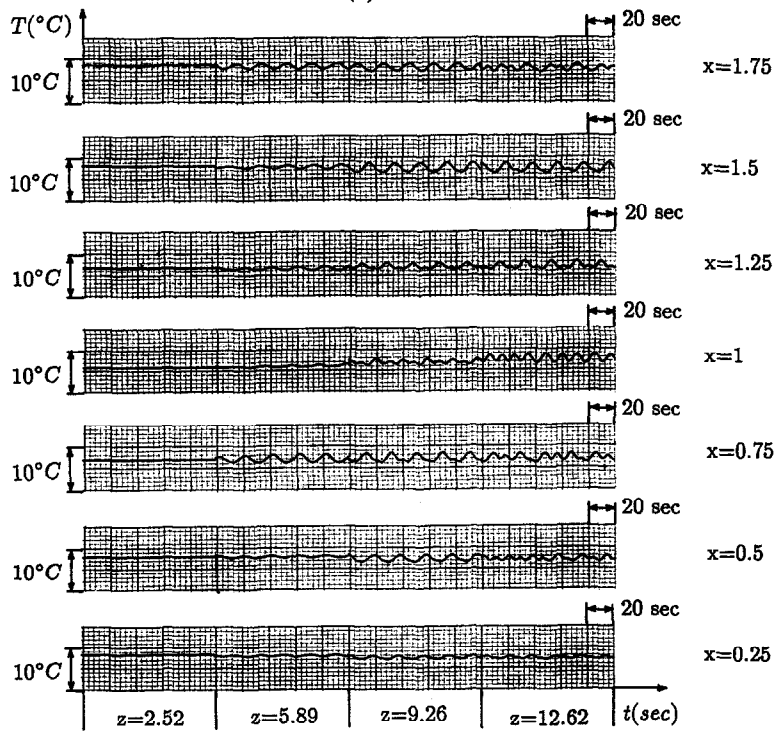


Fig. 13. Spatial-temporal structure of vortex flow: (a) top view photos at  $y = 0.5$ ; and (b) time records of air temperature at selected locations on lines  $y = 0.5$  and  $x = 2, 1.5, 1.0$  and  $0.5$  for  $A = 4$ ,  $Re = 20$  and  $Ra = 20,000$  ( $t_p = 5.6$  s).

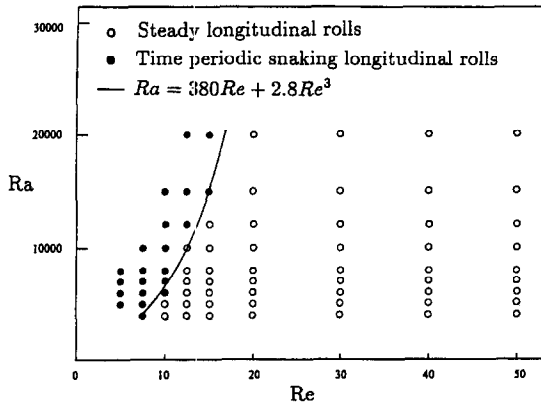
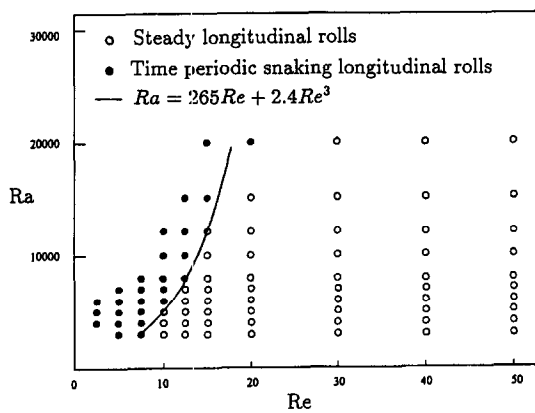


(a)



(b)

Fig. 14. Spatial-temporal structure of vortex flow : (a) top view photos at  $y = 0.5$  ; and (b) time records of air temperature at selected locations on lines  $y = 0.5$  and  $x = 1.75, 1.5, 1.25, 1, 0.75, 0.5$  and  $0.25$  for  $A = 2$ ,  $Re = 5$  and  $Ra = 5000$  ( $t_p = 20$  s).

(a)  $A=2$ (b)  $A=4$ Fig. 15. Flow regime maps delineating the steady and time periodic flows for: (a)  $A = 2$ ; and (b)  $A = 4$ .

## REFERENCES

- Mori, Y. and Uchida, Y., Forced convective heat transfer between horizontal flat plates. *International Journal of Heat and Mass Transfer*, 1966, **9**, 803-817.
- Nakayama, W., Hwang, G. J. and Cheng, K. C., Thermal instability in plane poiseuille flow. *Journal of Heat Transfer*, 1970, **92**, 61-68.
- Hwang, G. J. and Cheng, K. C., Convective instability in the thermal entrance region of a horizontal parallel-plate channel heated from below. *Journal of Heat Transfer*, 1973, **95**, 72-77.
- Lee, F. S. and Hwang, G. J., Transient analysis on the onset of thermal instability in the thermal entrance region of a horizontal parallel plate channel. *Journal of Heat Transfer*, 1991, **113**, 363-370.
- Ostrach, S. and Kamotani, Y., Heat transfer augmentation in laminar fully developed channel flow by means of heating from below. *Journal of Heat Transfer*, 1975, **97**, 220-225.
- Kamotani, Y. and Ostrach, S., Effect of thermal instability on thermally developing laminar channel flow. *Journal of Heat Transfer*, 1976, **98**, 62-66.
- Osborne, D. G. and Incropera, F. P., Experimental study of mixed convection heat transfer for transitional and turbulent flow between horizontal, parallel plates. *International Journal of Heat and Mass Transfer*, 1985, **28**, 1337-1344.
- Maughan, J. R. and Incropera, F. P., Regions of heat transfer enhancement for laminar mixed convection in a parallel plate channel. *International Journal of Heat and Mass Transfer*, 1990, **33**, 550-570.
- Chang, M. Y., Yu, C. H. and Lin, T. F., Changes of longitudinal vortex roll structure in a mixed convective air flow through a horizontal plane channel: an experimental study. *International Journal of Heat and Mass Transfer*, 1997, **40**, 347-363.
- Incropera, F. P. and Schutt, J. A., Numerical simulation of laminar mixed convection in the entrance region of horizontal rectangular duct. *Numerical Heat Transfer*, 1985, **8**, 707-729.
- Mahaney, H. V., Incropera, F. P. and Ramadhyani, S., Developing of laminar mixed convection flow in a horizontal rectangular duct with uniform bottom heating. *Numerical Heat Transfer*, 1987, **12**, 137-155.
- Mahaney, H. V., Incropera, F. P. and Ramadhyani, S., Effect of wall heat flux distribution on laminar mixed convection in the entrance region of a horizontal rectangular duct. *Numerical Heat Transfer*, 1988, **13**, 427-450.
- Hwang, C. C. and Lin, T. F., Buoyancy induced flow transition in mixed convective flow of air through a bottom heated horizontal rectangular duct. *International Journal of Heat and Mass Transfer*, 1994, **37**, 1235-1255.
- Luijckx, J. M. and Platten, J. K., On the existence of thermoconvective rolls transverse to a superimposed mean Poiseuille flow. *International Journal of Heat and Mass Transfer*, 1981, **24**, 1287-1291.
- Chiu, K. C., Ouazzani, J. and Rosenberger, R., Mixed convection between horizontal plates—II. Fully developed flow. *International Journal of Heat and Mass Transfer*, 1987, **30**, 1655-1662.
- Chiu, K. C. and Rosenberger, F., Mixed convection between horizontal plates—I. Entrance effects. *International Journal of Heat and Mass Transfer*, 1987, **30**, 1645-1654.
- Ouazzani, M. T., Caltagirone, J. P., Meyer, G. and Mojtabi, A., Etude numérique et expérimentale de la convection mixte entre deux plans horizontaux à températures différences. *International Journal of Heat and Mass Transfer*, 1989, **32**, 261-269.
- Ouazzani, M. T., Platten, J. K. and Mojtabi, A., Etude expérimentale de la convection mixte entre deux plans horizontaux à températures différence—II. *International Journal of Heat and Mass Transfer*, 1990, **33**, 1417-1427.
- Müller, H. W., Lücke, M. and Kamps, M., Transversal convection patterns in horizontal shear flow. *Physics Review A*, 1992, **45**, 3714-3726.
- Kline, S. J. and McClintock, F. A., Describing uncertainties in single-sample experiments. *Mechanical Engineering*, 1953, **75**, 3-12.
- Abernethy, R. B. and Thompson, J. W., Jr, Handbook—uncertainty in gas turbine measurements. Technical Report no. AEDC-TR-73-5 (AD-755356), March 1973.
- Shah, R. K. and London, A. L., *Laminar Flow Forced Convective in Ducts*. Academic Press, New York, 1987, pp. 196-198.